Electrical Power and Energy Systems 171 (2025) 110923

Contents lists available at ScienceDirect

International Journal of Electrical Power and Energy Systems

journal homepage: www.elsevier.com/locate/ijepes

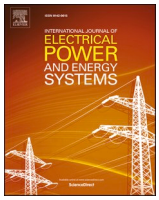

A holomorphic embedding power flow method based on dynamic power restart

Yi Zhang [a,*], Tian Lan [c], Chuandong Li [b,*], Weijie Cai [a], Zhiyu Lin [a]

[a] College of Electrical Engineering and Automation, Fuzhou University, Fuzhou, Fujian Province 350108, China
[b] College of Mechanical and Electrical Engineering, Fujian Agriculture and Forestry University, Fujian Province 350100, China
[c] State Grid Sanming Power Supply Company, Sanming, Fujian Province 365001, China

ARTICLE INFO

Keywords:
Analytical reconstruction
Dynamic power restart
Holomorphic embedding method

ABSTRACT

The holomorphic embedding method (HEM) is a newly developed recursive algorithm, which has the advantages of not depending on initial value selection and providing an analytical solution. However, in the actual power flow calculation of large power grids with heavy loads, HEM needs to calculate high-order power series coefficients, which is prone to numerical problems, resulting in convergence problems in power flow calculation. To improve the convergence characteristics of HEM, this paper proposes a holomorphic embedding power flow method based on dynamic power restart (DPRHEM). This method is based on the initial value flexibility of the fast and flexible holomorphic embedding power flow method (FFHEM) and incorporates the proposed dynamic update restart mechanism based on changes in power residuals to dynamically update and transmit the "germ" of the holomorphic embedding power flow method. It restricts the power series coefficients of the analytic function to low orders, so that the power state constantly approaches the target power state and ensures stable and reliable convergence during power flow calculation in large power grids with heavy loads. To a certain extent, this improves the efficiency of power flow calculation. Finally, this paper compares the performance of NRM, HEM and other restart-based HEMs on the case9 and case13659pegase systems of matpower8.0b1, as well as the actual East China regional power grid. The results show that DPRHEM has better convergence and higher computational efficiency in large power grids with heavy loads.

1. Introduction

Power flow calculation is the foundation of power system operation and planning [1–4]. With the access of new energy, the uncertainty of new energy brings new challenges to power system operation planning [5,6]. Some studies have proposed a series of new power flow methods for the uncertainty of new energy [7,8]. Currently, common power flow calculation methods are mainly based on the principle of numerical iteration, such as the Newton-Raphson method (NRM) [2,3] and the fast-decoupling method (FDM) [4]. However, NRM has some problems, such as initial guess dependence and poor convergence performance in ill-conditioned power flow [9–11]. Although FDM reduces the computational storage requirements compared with NRM, it is limited in dealing with distribution network or transmission and distribution joint network with large impedance due to the simplified requirements of the method [4].

The holomorphic embedding method (HEM) power flow method is widely used due to its insensitivity to initial values and its reliable convergence to the system's operational solution [12–20]. In [13] and [14], HEM is applied to the calculation of uncertain power flow and energy flow, respectively, and uses the characteristics of HEM analytical solution to realize the rapid analysis of power flow and energy flow in a large number of complex scenarios in the power system and integrated distribution power and heating system. Ref. [15] proposes a dynamic layer based on HEM to efficiently and stably generate fully operable control decisions for optimal power flow. To address the operational characteristics of AC, DC and converter stations in AC/DC hybrid power grids, the HEM power flow method tailored for AC/DC hybrid power grids is proposed in [16–18]. Some researchers have also developed applications for analyzing voltage collapse detection [19] or total transfer capability [20] based on the HEM concept. Current research on HEM in power flow analysis of AC/DC hybrid heavy-load large-scale power systems [21–23] and prediction of saddle bifurcation points on P-V curves [24,25] shows that the "germ" of HEM is related to its accuracy and convergence efficiency. With the increase of the complexity of the

* Corresponding authors.
E-mail addresses: zhangyi@fzu.edu.cn (Y. Zhang), lichuandong@126.com (C. Li).

https://doi.org/10.1016/j.ijepes.2025.110923
Received 6 March 2025; Received in revised form 11 July 2025; Accepted 16 July 2025
Available online 6 August 2025
0142-0615/© 2025 The Author(s). Published by Elsevier Ltd. This is an open access article under the CC BY-NC license (http://creativecommons.org/licenses/by-nc/4.0/).

Nomenclature

Abbreviations

HEM	Holomorphic embedding method
DPRHEM	Holomorphic embedding power flow method based on dynamic power restart
FFHEM	Fast and flexible holomorphic embedding power flow method
NRM	Newton-Raphson method
FDM	Fast-decoupling method
RHELM	Restarted holomorphic embedding load flow method

List of symbols

$x(s)$	Complex variable function
s	Complex variable (Holomorphic embedding factor)
$x[n]$	n-th order coefficient of the power series expansion of $x(s)$
N	Total number of system bus
i and k	Bus number
$Q_i(s)$	Reactive holomorphic function of bus numbered i
$V_i(s)$	Voltage holomorphic function of bus numbered i, $V_k(s)$ is the same
$W_i(s)$	Reciprocal of $V_i(s)$, $W_k(s)$ is the same
$V_i[n]$	n-th order coefficient of the power series expansion of $V_i(s)$; $V_k[n]$, $W_i[n]$, $W_k[n]$ and $Q_i[n]$ are the same
Y_{ik}	Element of the i-th row and the k-th column in the node admittance matrix $\boldsymbol{Y}$
$Y_{ik,tr}$	Line admittance part of Y_{ik}
$Y_{ik,sh}$	Ground admittance part of Y_{ik}
S_i	Complex power of bus i (Target state power)
P_i	Active power of bus i (Target state power)
V_i^{sp}	Specified voltage value for bus i
$\lvert V_i^{sp}\rvert$	Voltage amplitude of specified voltage value for bus i
V_{i0} and V_{k0}	Initial voltage value for bus i and k, which is an element of the initial voltage solution set V_{i0}
$\overline{*}$	Conjugate form of the variable *
V_{in} and V_{kn}	Truncated voltage of variable function $V_i(s)$ and $V_k(s)$ when $s = 1$ at n-th order, which is an element of the truncated voltage solution set V_{in}
S_{i0} and P_{i0}	Initial state power of S_i and P_i
S_{id} and P_{id}	Direction correction power of S_i and P_i
ΔS	Maximum power residual value
ΔS_n	ΔS when the power series coefficient is calculated to the n-th order
r	Convergence radius
ε	Set convergence precision
$\max(\cdot)$	Maximum value of the variable
$\min(\cdot)$	Minimum value of the variable
$f_{angle}(\cdot)$	Calculates the phase angle of the variable
V_{SL}^{sp}	Slack bus specified voltage
$\mathrm{Re}(\cdot)$ and $\mathrm{Im}(\cdot)$	Real and imaginary part extraction function, the superscripts Re and Im represent the real and imaginary part of the variable
δ_{n0} and δ_{n1}	Impulse functions activated only when $n = 0$ and $n = 1$
G_{ik} and B_{ik}	Real and imaginary parts of Y_{ik}
n	Order
m	Number of restarts

new power system network, the good "germ" of HEM becomes more difficult to obtain, and the poor "germ" easily leads to the need for high-order power series coefficient calculation of HEM [22]. When classical HEM transforms the power flow problem into a linear matrix problem, as the order of the coefficients to be solved increases, it is prone to numerical instability [26]. The analytical continuation is easily affected by the bifurcation point and blocked. The linear matrix problem is easy to become ill-conditioned, and the power flow is difficult to converge [26–31]. Therefore, it is necessary to obtain high-quality "germ" through multi-stage prediction correction to improve the convergence performance of HEM.

On the other hand, the analysis of the analytical solutions derived from the HEM in [32] reveals increasing the order of power series calculation results in a denser zero-pole distribution of the analytical solution. This distribution can obstruct the analytical continuation path, resulting in slow or even problematic convergence. References [26,33] analyze the analytical continuation process of the HEM power flow method and indicate that the high-order power series calculations might introduce a pseudo zero-pole pair (Froissart doublets' effects) into the Padé approximation, which adversely affects power flow convergence. In order to address these issues, [21] proposes a fast and flexible HEM (FFHEM) power flow method, which allows for a flexible configuration of its initial voltage solution to reduce the solution order and shorten the solution time. However, this approach sacrifices the initial value insensitivity of the HEM power flow method, potentially worsening convergence when initial value predictions are unreasonable. Based on [21,24] proposed a method to analyze the static stability of large-scale power systems by piecewise approximation. The method realizes the evaluation and piecewise approximation of the solution through the preset initial interval $[s_a, s_b]$, the initial interval length $\Delta s = s_b\text{-}s_a$, order limit q, but the approximation effect of this method depends on the preset value. Moreover, [22] introduced a restarted holomorphic embedding load flow method (RHELM), which sets a fixed-order restart mechanism to update the voltage state, so as to reduce the time that HEM takes to solve the power flow calculations. The [23] defined a convergence factor to determine the restart of the model according to the value of the convergence factor, thereby reducing the total calculation time. the settings of the above two restart methods are heuristic, and the settings of the restart order N_R (N_0) in [22] and the convergence factor upper limit δ^M in [23] cannot be dynamically adapted. As such, the convergence effect of the restart mechanism cannot be guaranteed, which limits its application scenarios.

To address the convergence issues of the HEM power flow method in large power grids under heavy load conditions, this paper proposes DPRHEM. The proposed method builds upon the initial value flexibility of the FFHEM proposed in [21] to divide the power in the HEM power flow model into the initial state power and the direction correction power. By relaxing the power state, the DPRHEM constructs a model capable of dynamically updating and transferring the "germ" and correcting the analytical direction. The compact form of the power series coefficient calculation matrix equation is then generated. In terms of the restart mechanism of recursive solutions, the proposed method establishes a dynamic update restart criterion based on changes in power residual, which makes the initial state power quickly approach the target state power. This improves the convergence rate of the method and limits the power series coefficients of the analytical function to low orders, avoids convergence issues caused by high-order calculations [24], and ensures stable and reliable convergence during power flow calculation in large power grids with heavy loads.

The primary contributions of this paper are as follows:

1) The proposed DPRHEM realizes the complementarity of the advantages and disadvantages of classical HEM and FFHEM based on the dynamic restart mechanism of maximum power residual, which effectively resolves the poor convergence issues of the classical HEM in actual large-scale and heavily loaded power flow calculations.

2) The importance of restart timing for HEM convergence performance is demonstrated. The restart mechanism of the proposed DPRHEM dynamically changes the restart conditions and a physically meaningful solution can be obtained under the restart constraint, which greatly guarantees the reliability of the convergence results of the proposed method.
3) The DPRHEM adjusts the analytical function by dynamic power restart, expands the convergence radius of the function, and ensures that the power flow solution finally resides within the convergence domain. The proposed method does not need Padé approximation, which reduces the computational cost significantly.

The remainder of the paper is organized as follows. Section II describes the fundamental principles of HEM and the applicability of three primary forms of HEM. Section III introduces the DPRHEM and the corresponding dynamic power restart mechanism. Section IV compares the performance of the DPRHEM with NRM, classical HEM and RHELM on several systems. Section V provides the conclusion.

2. HEM power flow method

2.1. Fundamental principles of HEM

According to the definition of a holomorphic function, a complex variable function $x(s)$ is termed holomorphic if it satisfies the Cauchy-Riemann equation and is differentiable in the neighborhood U of a certain point, which allows $x(s)$ to be expressed as a power series in the complex field U as shown in formula (1).

$$x(s) = \sum_{n=0}^{\infty} x[n]s^n \tag{1}$$

For the nonlinear power flow equation $f(x) = 0$, which presents computational challenges, the variable x (including bus voltage and generator reactive power) can be modeled as a holomorphic function in the form of (1). This function is then embedded into the nonlinear power flow equation to obtain the holomorphic embedded power flow equation $f(x) = f[x(s)] = 0$. By equating the power series coefficients of the corresponding orders on both sides of the equation, a recursive relationship is derived, from which the coefficient $x[n]$ for each order is obtained. This process obtains the analytical expression for the variable x to be solved.

When constructing holomorphic embedded power flow equations, it is necessary to ensure that the following four basic conditions are satisfied [34]:

1) The function $x(s)$ must remain holomorphic in $f[x(s)] = 0$.
2) For the holomorphic embedded power flow equation $f[x(s)] = 0$ at $s = 0$, the solution $x(0)$ has a practical physical meaning and is easy to obtain.
3) For the holomorphic embedded power flow equation $f[x(s)] = 0$ at $s = 1$, $f[x(1)] = 0$ should correspond exactly to the original nonlinear power flow equation $f(x) = 0$, making $x(1)$ the definitive solution.
4) Along the s path before the saddle-node bifurcation point, the holomorphic embedded power flow equation $f[x(s)] = 0$ should not encounter any additional saddle-node bifurcation points, ensuring that $f[x(s)]$ is continuous and unimpeded in the analytical continuation process of *s* from 0 to 1.

2.2. Applicability analysis of HEM power flow method

When constructing the HEM power flow equation, four basic conditions of holomorphic embedding need to be satisfied. The embedding factor s needs to be reasonably embedded in the original power flow equation to ensure that the HEM model has physical meaning in the initial state and can be accurately reverted to the original power flow equation problem in the target state. At present, there are three primary forms of holomorphic embedding utilized in HEM power flow methods are shown in Table 1.

1) Traditional HEM [35]: The embedding factor s has a specific physical meaning and can be used as the scaling factor for the injected node power, which represents the load level of the system. However, the initial solution of the algorithm is single and needs to be calculated. Moreover, the method cannot guarantee convergence to physically meaningful solution.
2) Classical HEM [12]: This method has a clear and easily obtainable initial solution corresponding to the no-load state of the system when $s = 0$ and ensures that the method's final convergence result is a high-voltage solution. However, when dealing with the case of large systems and heavy loads, this method generally requires high-order power series calculation, which is prone to numerical instability. This can lead to convergence oscillations or stagnation solutions in the solution process.
3) FFHEM [21]: This method can flexibly configure its initial solution with any state serving as the initial state, thus enhancing its potential for integration with other power flow methods. However, this method cannot always guarantee the suitability of the selected initial solution. The convergence depends on the configured initial solution.

In summary, it is evident that the current HEM power flow methods still necessitate optimization and improvements in terms of numerical convergence range. The method in this paper combines the advantages of FFHEM's flexible configuration of initial solutions with the advantages of classical HEM's simple acquisition of reliable initial solutions by proposing a restart mechanism to solve the convergence problem of large systems and heavy loads and improve the computational efficiency of the algorithm.

3. HEM based on dynamic power restart

The radius of the approximate circle formed by the zero-pole pair of the analytic function of the holomorphic embedding model can be defined as the convergence radius r, which reflects the convergence performance of the model [12,30]. When r is more than 1, the model can converge quickly. When r is less than 1, the model cannot converge. When r is close to 1, the model is difficult to converge. Fig. 1 shows that the proposed method is based on the characteristics that FFHEM can flexibly configure its initial solution. The model truncation is controlled by the restart mechanism to obtain physically meaningful voltage solution V_{in} (Truncated voltage solution of variable function $V_i(s)$ when $s = 1$ at *n*-th-order) within the convergence radius. Then use it as the "germ" V_{i0} of the restarted and updated model, and uses the (2) to obtain the corresponding initial state power $S_{i0}(P_{i0})$ and direction correction power S_{id} (P_{id}), finally realize the model update. The S_{id} (P_{id}) can characterize the distance between the $S_{i0}(P_{i0})$ and the target state power $S_i(P_i)$ after the model update [36,37]. Thus, $S_{i0}(P_{i0})$ and $S_i(P_i)$ represent the bus injection power of "germ" and the target solution, respectively. This model construction method can analyze the distance between $S_{i0}(P_{i0})$ and S_i (P_i) of the model, helps to update the model to expand the convergence radius of the analytical function, and improves the convergence performance of the method, which has universal applicability.

Table 1
Three Standard HEM Forms.

Traditional HEM [35]	PQ bus	$\sum_{k=1}^{N} Y_{ik}V_k(s) = \frac{s\overline{S_i}}{\overline{V_i}(\bar{s})}$
	PV bus	$\sum_{k=1}^{N} Y_{ik}V_k(s) = \frac{sP_i\text{-}jQ_i(s)}{\overline{V_i}(s)}$ $V_i(s)\overline{V_i}(s) = \lvert V_i^{sp}\rvert^2$
	SL bus	$V_i(s) = V_i^{sp}$
Classical HEM [12]	PQ bus	$\sum_{k=1}^{N} Y_{ik,tr}V_k(s) = \frac{s\overline{S_i}}{\overline{V_i}(s)} - Y_{ik,sh}V_i(s)$
	PV bus	$\sum_{k=1}^{N} Y_{ik,tr}V_k(s) = \frac{sP_i\text{-}jQ_i(s)}{\overline{V_i}(s)} - sY_{ik,sh}V_i(s)$ $V_i(s)\overline{V_i}(\bar{s}) = 1 + s\left(\lvert V_i^{sp}\rvert^2\text{-}1\right)$
	SL bus	$V_i(s) = 1 + s\left(V_i^{sp}\text{-}1\right)$
FFHEM [21]	PQ bus	$\overline{V}_i(\bar{s})\sum_{k=1}^{N} Y_{ik}V_k(s) = \overline{V}_{i0}\sum_{k=1}^{N} Y_{ik}V_{k0} + s\left(\overline{S}_i\text{-}\overline{V}_{i0}\sum_{k=1}^{N} Y_{ik}V_{k0}\right)$
	PV bus	$\overline{V}_i(\bar{s})\sum_{k=1}^{N} Y_{ik}V_k(s) + V_i(s)\sum_{k=1}^{N} \overline{Y}_{ik}\overline{V}_k(\bar{s}) =$ $\left(\overline{V}_{i0}\sum_{k=1}^{N} Y_{ik}V_{k0} + V_{i0}\sum_{k=1}^{N} \overline{Y}_{ik}\overline{V}_{k0}\right) + s\left(2P_i\text{-}\left(\overline{V}_{i0}\sum_{k=1}^{N} Y_{ik}V_{k0} + V_{i0}\sum_{k=1}^{N} \overline{Y}_{ik}\overline{V}_{k0}\right)\right)$ $V_i(s)\overline{V}_i(\bar{s}) = V_{i0}\overline{V}_{i0} + s\left(\lvert V_i^{sp}\rvert^2\text{-}V_{i0}\overline{V}_{i0}\right)$
	SL bus	$V_i(s) = V_i^{sp}$

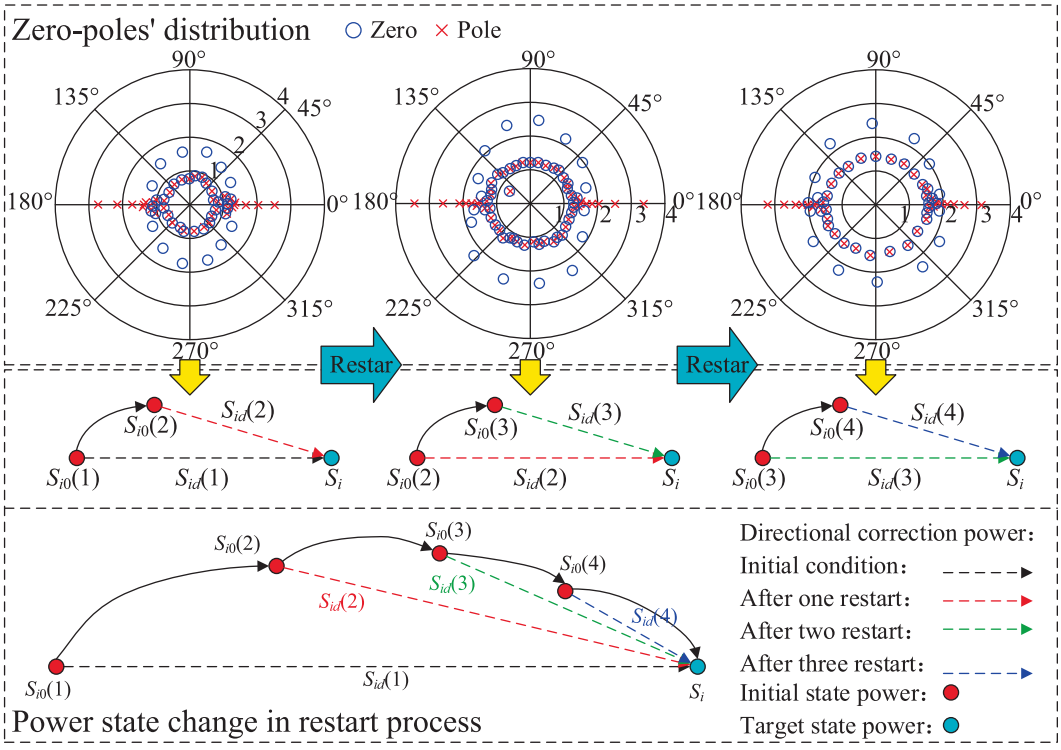

Fig. 1. The schematic diagram of the proposed method.

$$\begin{cases} S_{i0} = V_{i0}\sum_{k=1}^{N} \overline{Y}_{ik}\overline{V}_{k0} \\ S_{id} = S_i\text{-}S_{i0} \\ i \in PQ \end{cases} \quad \begin{cases} P_{i0} = \mathrm{Re}\left(V_{i0}\sum_{k=1}^{N} \overline{Y}_{ik}\overline{V}_{k0}\right) \\ P_{id} = P_i\text{-}P_{i0} \\ Q_i[0] = \mathrm{Im}\left(V_{i0}\sum_{k=1}^{N} \overline{Y}_{ik}\overline{V}_{k0}\right) \\ i \in PV \end{cases} \tag{2}$$

Here $Q_i[0]$ indicates the reactive power at the initial state.

3.1. Model construction

Based on (2), the DPRHEM model for PQ buses is established:

$$\sum_{k=1}^{N} Y_{ik}V_k(s) = \frac{\overline{S}_{i0} + s\overline{S}_{id}}{\overline{V}_i(\overline{s})} \tag{3}$$

Since the constructed holomorphic embedding power flow equation needs to adhere to the Cauchy-Riemann conditions, the holomorphic embedding form for the voltage conjugate $\overline{V}(\overline{s})$ must satisfy the following conditions [29]:

$$\overline{V}(\overline{s}) = \sum_{n=0}^{\infty} \overline{V}[n]s^n \tag{4}$$

where $\overline{V}[n]$ is the conjugate of $V[n]$ and $V[n]$ is the nth-order coefficient of the analytic function $V(s)$.

To better analyze the reactive power change of PV bus, this paper constructs the following DPRHEM model for PV buses:

$$\begin{cases} \sum_{k=1}^{N} Y_{ik}V_k(s) = \dfrac{P_{i0} + sP_{id}\text{-}jQ_i(s)}{\overline{V}_i(s)} \\ V_i(s)\overline{V}_i(s) = V_{i0}\overline{V}_{i0} + s\left(\left|V_i^{sp}\right|^2\text{-}V_{i0}\overline{V}_{i0}\right) \end{cases} \tag{5}$$

The construction of the model retains the holomorphic analytical function $Q(s)$ for the reactive power at the PV bus. This form is convenient to directly analyze the change of the reactive power state of the PV bus through the analytical function and provides the basis for the strategic switching of reactive power devices. At the same time, this model leaves space for considering reactive power in the restart mechanism in the future.

The slack bus model is as follows:

$$V_i(s) = V_{i0} + s\left(V_i^{sp}\text{-}V_{i0}\right) \tag{6}$$

From (2) to (6), it is evident that the power flow model in the proposed method can be equivalent to FFHEM by conjugate symmetry processing and matrix change when restart is not considered. The model shows the restart mechanism in the power injection space and retains the ability of FFHEM to start flexibly from any state, which provides a foundational framework for the application of the restart mechanism.

3.2. Dynamic power restart mechanism

Building on the above model, this paper introduces a restart mechanism. During recursive calculations of the HEM model, after each next-order power series coefficient (such as $V_i[n]$) is calculated, the obtained analytic function $V_i(s)$ can be truncated and the numerical solution V_{in} can be obtained at $s = 1$. Then the maximum power residual ΔS_n of the model at this time can be calculated by (7). We note that the value of ΔS_n is the basis for judging whether the power flow converges and the change trend of ΔS reflects the change of the distance of bus injection power during the analytic continuation of the HEM, which can be served as a criterion for deciding whether to continue recursive calculations or to perform a restart. Therefore, combining the restart mechanism based on the change trend of ΔS with the HEM demonstrates strong theoretical adaptability.

$$\Delta S_n = \max\begin{Bmatrix} \mathrm{abs}(V_{in}\sum_{k=1}^{N} Y_{ik}\overline{V}_{kn} - S_i) & i \in PQ\ \mathrm{bus} \\ \mathrm{abs}(\mathrm{real}(V_{in}\sum_{k=1}^{N} Y_{ik}\overline{V}_{kn} - S_i)) & i \in PV\ \mathrm{bus} \\ \mathrm{abs}(|V_i^{sp}| - |V_{in}|) & i \in PV\ \mathrm{bus} \end{Bmatrix} \tag{7}$$

where ΔS_n represents the maximum power residual value obtained after the calculation of the n-th-order power series coefficient of the model. The voltage V_{in} represents the voltage function $V_i(s)$ is calculated to the n-th order coefficient and the value of $s = 1$ is taken, i.e., $V_{in} = \sum_{t=0}^{n} V_i[t]$, V_{kn} is the same as it.

According to the principle of HEM, it can be known that when the "germ" of HEM (corresponding to the initial state power $S_{i0}(P_{i0})$) is a physically meaningful solution, the power flow solution obtained within the convergence radius is also a physically meaningful solution [12,13]. Thus, the choice of the initial state transmitted during the update of the DPRHEM model is crucial. In order to ensure that the initial state power is easily accessible and the "germ" is physically meaningful, this paper utilizes the classical HEM as the starting model. When the classical HEM analyzes the power flow of the power system, the change of ΔS has the following two phenomena:

1) In well-conditioned systems [38,39] the load is normal and the ΔS of the power flow tends to decrease with an increase in the order of the power series [30], as shown in Fig. 2.
2) In ill-conditioned systems [39,40], the network is complex, the load is heavy, and the nonlinearity of power flow calculation is enhanced [38]. With the increase of HEM power series calculation order, the analytic function approximation of HEM is limited by the size of the convergence radius r and becomes difficult to converge. When $r \approx 1$, the high-order coefficients cannot accurately represent the characteristics of the analytical function, the analytical function is difficult to be fitted, and ΔS is prone to stagnation. When $r < 1$, the branch-cut line formed by the zero-pole pair of the analytical function hinders the analytical continuation from $s = 0$ to $s = 1$, which is prone to induce the numerical problem of function approximation, and ΔS is prone to diverge. The stagnation trend and divergence trend of ΔS are depicted in Fig. 3.

In view of the above phenomenon, this paper takes the relationship between the change of ΔS after each recursive calculation and the set convergence precision ε as a criterion for decision-making, and proposes

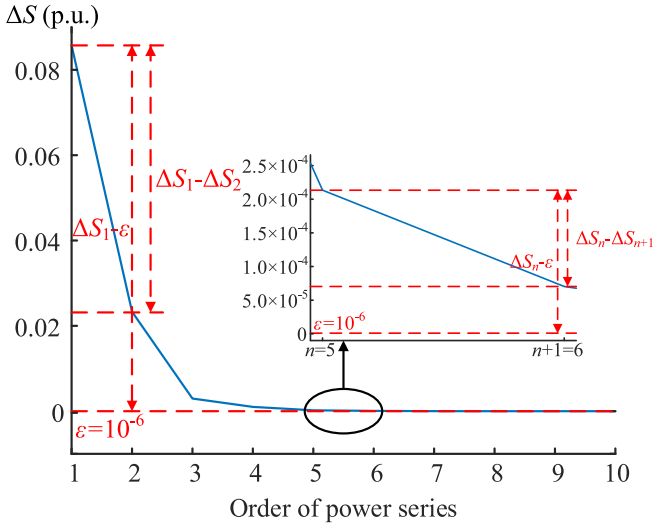

Fig. 2. Convergence trends of ΔS in the HEM.

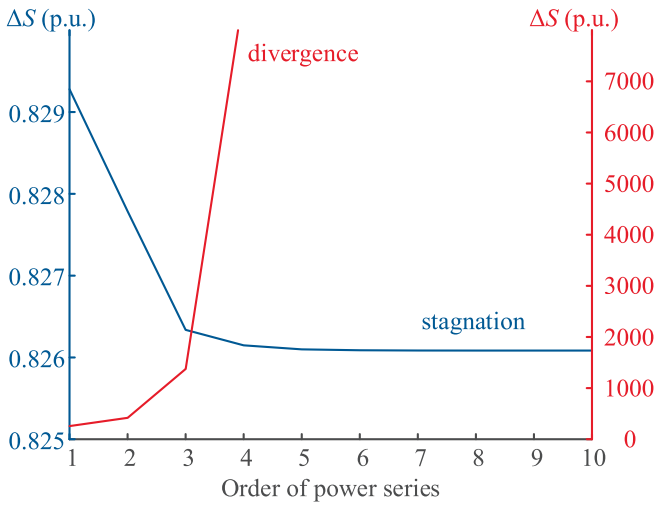

Fig. 3. Divergence and stagnation trends of ΔS in the HEM.

a restart mechanism in two aspects. One is used to deal with the problem of slow convergence and stagnation solution, and the other is used to deal with the divergence problem. It is stated here that for well-conditioned small systems, the convergence of the HEM typically requires a low order of power series, allowing it to achieve convergence before the convergence rate decreases, without restart or only one restart.

In ill-conditioned systems, when the problem of slow convergence or stagnation solution occurs, if ΔS still tends to decrease with the increase of the power series coefficient order, we can consider that the function approximation is still within the convergence radius [30]. At this point, if a certain change process of ΔS satisfies (8), the voltage solution V_{in} obtained by truncating the analytic function at $s = 1$ is used as the initial voltage solution V_{i0}. Thus, V_{i0} can be considered a physically meaningful solution. After obtaining the initial voltage solution V_{i0}, the initial state power $S_{i0}(P_{i0})$ and the direction correction power $S_{id}(P_{id})$ of each bus are obtained by (2) to realize the restart and update of the model.

$$\frac{\Delta S_1-\Delta S_2}{\Delta S_1-\varepsilon} \geq \frac{\Delta S_{n-1}-\Delta S_n}{\Delta S_{n-1}-\varepsilon} > 0 \tag{8}$$

In the power injection space, DPRHEM can continuously make ΔS approach ε through restart and recursive calculation. Here we use the quotient convergence theorem [41], set $(\Delta S_{n-1}-\Delta S_n)/(\Delta S_{n-1}-\varepsilon)$ as the evidence for judging the convergence speed, and $(\Delta S_1-\Delta S_2)/(\Delta S_1-\varepsilon)$ as the critical value of the convergence speed restart constraint. According to the quotient convergence theorem [41]: Let two adjacent iterative points: x_{k-1}, x_k, the optimal value point x^*, if there is a real number $q > 0$, satisfying (9), if $0 < q < 1$, then the algorithm is linear convergence; if $q = 1$, it represents the sublinear convergence of the algorithm; if $q = 0$, the algorithm is superlinearly convergent.

$$\lim_{k\to\infty}\frac{\|x_k-x^*\|}{\|x_{k-1}-x^*\|} = q \tag{9}$$

Then $(\Delta S_{n-1}-\Delta S_n)/(\Delta S_{n-1}-\varepsilon)$ in (8) can be changed to (10). Combined with the above definition of convergence rate, ε, ΔS_{n-1} and ΔS_n can be regarded as x^*, x_{k-1} and x_k respectively.

$$\frac{\Delta S_{n-1}-\Delta S_n}{\Delta S_{n-1}-\varepsilon} = 1-\frac{\Delta S_n-\varepsilon}{\Delta S_{n-1}-\varepsilon} \tag{10}$$

Combined with the definition of quotient convergence, it can be seen that when $(\Delta S_n-\varepsilon)/(\Delta S_{n-1}-\varepsilon)$ is closer to 0 (i.e., when $(\Delta S_{n-1}-\Delta S_n)/(\Delta S_{n-1}-\varepsilon)$ is larger and closer to 1), the proposed method is closer to superlinear convergence and the convergence speed is faster. Based on this feature, and considering that the approximation effect of HEM in Fig. 2 is most obvious in the first recursive calculation to the second recursive calculation, the proposed restart mechanism sets $(\Delta S_1-\Delta S_2)/(\Delta S_1-\varepsilon)$ as the critical value of the convergence speed restart constraint. At the same time, $(\Delta S_1-\Delta S_2)/(\Delta S_1-\varepsilon)$ can have different values according to different operating conditions of different systems, which can make the constraint condition (8) more universal. Therefore, the proposed restart mechanism has better dynamic response characteristics and universal characteristics. Compared with the restart mechanism in Reference [22], it can adapt to more operating conditions of more systems. Compared with the restart mechanism in Reference [23], it can solve the problem of stagnation solution or slow convergence of power flow more effectively.

In ill-conditioned systems, when the divergence problem occurs, ΔS diverges, and the analytical continuation of the model may shuttle around the boundary of the convergence domain, which may cause the voltage solution V_{in} truncated at $s = 1$ in the function approximation process to be a physically meaningless solution. If a restart occurs under such conditions, the power flow solution may erroneously transition from a branch of physically meaningful solutions to one that is physically meaningless, and the power flow cannot reliably converge. Such physically meaningless solutions are usually characterized by very large phase angles [42,43]. Therefore, we propose another condition of the restart strategy. When ΔS diverges, indicated by the relationship in (11), the phase angle difference between the voltage solution V_{in} (i.e., the initial voltage solution V_{i0} of the restart update model) obtained by the analytical function truncation at $s = 1$ and the slack bus voltage needs to satisfy the constraint. The constraint conditions are expressed by (12). When (12) is satisfied, the obtained truncated voltage solution V_{in} is regarded as a physically meaningful solution. Only then will the model be updated and restarted.

$$\frac{\Delta S_{n-1}-\Delta S_n}{\Delta S_{n-1}-\varepsilon} < 0 \tag{11}$$

$$\begin{cases} \max\left(f_{angle}(V_{i0})-f_{angle}(V_{SL}^{sp})\right) < 90^o \\ \min\left(f_{angle}(V_{i0})-f_{angle}(V_{SL}^{sp})\right) > -90^o \end{cases} \tag{12}$$

The phase angle constraint (12) is set in this paper to avoid that the "germ" transmitted to the restarted model when diverging are physically meaningless solutions. The upper and lower limits are set to ± 90°, based on optimal numerical results derived from multiple numerical experiments (The constraint range with a value less than 90° is too conservative. The robustness of the constraint range more than 90° is poor.). Some bus voltages may exhibit a phase angle offset through transformers, which can be superimposed to the upper and lower limits of the constraint for appropriate adjustments. The proposed constraint condition (12) can greatly ensure that the "germ" transmitted to the restart model is a physically meaningful solution, so as to ensure the reliability of the power flow convergence result. The convergence performance of the proposed method is better than the classical HEM, NRM and RHELM, which can meet basic engineering application requirements. However, the proposed method cannot prove the selection of the constraint condition limit from the mathematical principle for the time being. In the future, it is expected to enhance the interpretability of the restart mechanism through more comprehensive theoretical research.

In summary, if the initial change in ΔS shows an increasing trend, it is judged whether to restart according to (12). If the restart condition (12) persistently is not satisfide, and ΔS decreases for the first time (assuming that it begins to decrease at the m-th order, i.e., $\Delta S_{m-1} - \Delta S_m > 0$), then the subsequent descent process is judged by (8) whether to restart, where only $(\Delta S_1-\Delta S_2)/(\Delta S_1-\varepsilon)$ on the left side of (8) needs to be modified as $(\Delta S_{m-1} - \Delta S_m)/(\Delta S_{m-1} - \varepsilon)$. The criterion alternates between (8) and (12) according to the change in ΔS.

From the perspective of power injection space, the restart mecha-

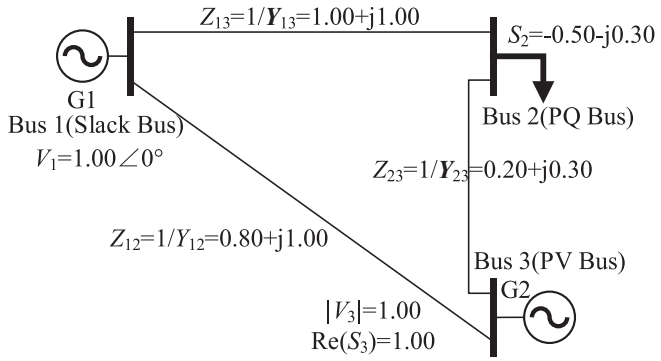

Fig. 4. A 3-bus system.

nism is designed based on the rate at which the initial state power $S_{i0}(P_{i0})$ approaches the target state power $S_i(P_i)$, providing a clear physical rationale. Although the restart makes the proposed method have iterative characteristic, according to the single-valued approximation characteristics of HEM and the constraint conditions of the restart mechanism of the proposed method, the initial state transmitted during the restart has practical physical meaning that can be guaranteed greatly, thereby guaranteeing the reliability of the convergence results. In addition, the restart mechanism restricts the method to the calculation of low-order power series, thereby avoiding the numerical stability issues in the calculations of high-order power series. Moreover, the numerical solution for the target state can be achieved by direct summation, eliminating the need for Padé approximation calculations and thus considerably reducing the computational cost of the method.

3.3. Model solving

The recursive calculation matrix equation for each bus model of the proposed method can be derived according to the principle of equating power series coefficients. Detailed elaboration and clarification are presented in the following:

1) Slack Bus

Eq. (13) models the voltage of the slack bus:

$$\begin{bmatrix} 1 & 0 \\ 0 & 1 \end{bmatrix} \begin{bmatrix} V_i^{Re}[n] \\ V_i^{Im}[n] \end{bmatrix} = \begin{bmatrix} \mathrm{Re}\left(\delta_{n0} V_{i0} + \delta_{n1}\left(V_i^{sp}\text{-}V_{i0}\right)\right) \\ \mathrm{Im}\left(\delta_{n0} V_{i0} + \delta_{n1}\left(V_i^{sp}\text{-}V_{i0}\right)\right) \end{bmatrix} \tag{13}$$

where Re(·) is a real part function and Im(·) is the imaginary part function. The superscripts Re and Im represent the real and imaginary parts of the variable, respectively. δ_{n0} and δ_{n1} are impulse functions activated only when $n = 0$ and $n = 1$, respectively.

2) PQ Bus

Equation (14) relates to PQ buses:

$$\sum_{k=1}^{N} \left(\begin{bmatrix} G_{ik} & -B_{ik} \\ B_{ik} & G_{ik} \end{bmatrix} \begin{bmatrix} V_k^{Re}[n] \\ V_k^{Im}[n] \end{bmatrix} \right) = \begin{bmatrix} \mathrm{Re}(K[n\text{-}1]) \\ \mathrm{Im}(K[n\text{-}1]) \end{bmatrix} - \begin{bmatrix} \mathrm{Re}\left(\overline{S}_{i0}(\overline{W}_i[0])^2\right) & \mathrm{Im}\left(\overline{S}_{i0}(\overline{W}_i[0])^2\right) \\ \mathrm{Im}\left(\overline{S}_{i0}(\overline{W}_i[0])^2\right) & -\mathrm{Re}\left(\overline{S}_{i0}(\overline{W}_i[0])^2\right) \end{bmatrix} \begin{bmatrix} V_i^{Re}[n] \\ V_i^{Im}[n] \end{bmatrix} \tag{14}$$

where G_{ik} and B_{ik} are the real and imaginary parts of Y_{ik}, which represent the conductance and susceptance between bus i and bus k. The auxiliary variable K[n-1] is defined as:

$$K[n\text{-}1] = \overline{S}_{id}\overline{W}_i[n\text{-}1] - \overline{S}_{i0}\overline{W}_i[0] \sum_{t=1}^{n-1} (\overline{W}_i[t]\overline{V}_i[n\text{-}t]) \tag{15}$$

where $W_i[\cdot]$ denotes the power series coefficient $W_i(s)$ of the auxiliary holomorphic function, which is the reciprocal of $V_i(s)$. This reciprocal relationship facilitates the Taylor expansion of equations in the model where $V_i(s)$ appears in the denominator, which helps the model achieve linear recursive calculation and ensures the reliability of power flow convergence.

$$W_i(s) = \frac{1}{V_i(s)} = \sum_{n=0}^{\infty} W_i[n] s^n \tag{16}$$

3) PV Bus

Eq. (17) shows the relationship for PV buses

$$\sum_{k=1}^{N} \left(\begin{bmatrix} G_{ik} & -B_{ik} \\ B_{ik} & G_{ik} \end{bmatrix} \begin{bmatrix} V_k^{Re}[n] \\ V_k^{Im}[n] \end{bmatrix} \right) = \begin{bmatrix} \mathrm{Re}(L[n\text{-}1]) \\ \mathrm{Im}(L[n\text{-}1]) \end{bmatrix} - \begin{bmatrix} W_i^{Im}[n] \\ W_i^{Re}[n] \end{bmatrix} Q_i[n] - \begin{bmatrix} \mathrm{Re}(D[0]) & \mathrm{Im}(D[0]) \\ \mathrm{Im}(D[0]) & -\mathrm{Re}(D[0]) \end{bmatrix} \begin{bmatrix} V_i^{Re}[n] \\ V_i^{Im}[n] \end{bmatrix} \tag{17}$$

$$V_i^{Re}[n] = M[n\text{-}1] - (V_i^{Im}[0]/V_i^{Re}[0]) V_i^{Im}[n] \tag{18}$$

where $Q_i[n]$ is the *n*-order coefficient of the PV bus reactive power analytic function $Q_i(s)$. The auxiliary variables L[n-1], D[0] and M[n-1] are as defined follows:

$$\begin{cases} L[n\text{-}1] = P_{id}\overline{W}_i[n\text{-}1] - j\sum_{t=1}^{n-1} Q_i[t]\overline{W}_i[n\text{-}t] \\ \quad -(P_{i0}\text{-}jQ_i[0])\overline{W}_i[0]\sum_{t=1}^{n-1}\overline{W}_i[t]\overline{V}_i[n\text{-}t] \\ D[0] = (P_{i0}\text{-}jQ_i[0])(\overline{W}_i[0])^2 \\ M[n\text{-}1] = \left(\begin{matrix} \delta_{n0}(V_{i0})^2 + \delta_{n1}((V_i^{sp})^2\text{-}(V_{i0})^2)/2 \\ -\left(\sum_{t=1}^{n-1} V_i[t]\overline{V}_i[n\text{-}t]\right)/2 \end{matrix} \right) / V_i^{Re}[0] \end{cases} \tag{19}$$

Taking a 3-bus system shown in Fig. 4 as an illustrative example to demonstrate the integration of (13), (14), and (17) into a unified matrix equation calculation form. Firstly, we employ equation transformations and substitutions to replace the variable $V_k^{Re}[n]$ in the matrix equation with the expression in (18). Subsequently, we rearrange the equation to place the reactive power variables to be solved on the left side such that all unknown variables are on the left side and all known variables are on the right side. This reorganization facilitates the formulation of a linear equation $AX = b$, where A represents the coefficient matrix of the recursively computed linear equation that can be obtained, X denotes the vector of power series coefficients for the model waiting to be solved, and b is a known vector calculated using coefficients of order not higher than $n - 1$. The detailed expansion of this matrix equation is presented in (20). In this configuration, bus numbers 1, 2 and 3 correspond to variables i and k, which represent the slack bus, PQ bus and PV bus, respectively.

$$\begin{bmatrix} 1 & 0 & 0 & 0 & 0 & 0 \\ G_{21} & G_{22\_Re} & 0 & -B_{21} & -B_{22\_Re} & -B_{23}\text{-}\left(G_{23}V_3^{Im}[0]/V_3^{Re}[0]\right) \\ G_{31} & G_{32} & W_3^{Im}[0] & -B_{31} & -B_{32} & -B_{33\_Re}\text{-}\left(G_{33\_Re}V_3^{Im}[0]/V_3^{Re}[0]\right) \\ 0 & 0 & 0 & 1 & 0 & 0 \\ B_{21} & B_{22\_Im} & 0 & G_{21} & G_{22\_Im} & G_{23}\text{-}\left(B_{23}V_3^{Im}[0]/V_3^{Re}[0]\right) \\ B_{31} & B_{32} & W_3^{Re}[0] & G_{31} & G_{32} & G_{33\_Im}\text{-}\left(B_{33\_Im}V_3^{Im}[0]/V_3^{Re}[0]\right) \end{bmatrix} \begin{bmatrix} V_1^{Re}[n] \\ V_2^{Re}[n] \\ Q_3[n] \\ V_1^{Im}[n] \\ V_2^{Im}[n] \\ V_3^{Im}[n] \end{bmatrix} = \begin{bmatrix} \mathrm{Re}(\delta_{n0}V_{10} + \delta_{n1}(V_1^{sp}\text{-}V_{10})) \\ \mathrm{Re}(K[n\text{-}1]) - G_{23}M[n\text{-}1] \\ \mathrm{Re}(L[n\text{-}1]) - G_{33\_Re}M[n\text{-}1] \\ \mathrm{Im}(\delta_{n0}V_{10} + \delta_{n1}(V_1^{sp}\text{-}V_{10})) \\ \mathrm{Im}(K[n\text{-}1]) - B_{23}M[n\text{-}1] \\ \mathrm{Im}(L[n\text{-}1]) - B_{33\_Re}M[n\text{-}1] \end{bmatrix} \tag{20}$$

where the auxiliary variables G_{22_Re}, B_{22_Re}, G_{22_Im}, B_{22_Im}, G_{33_Re}, B_{33_Re}, G_{33_Im} and B_{33_Im} can be expressed as follows:

$$\begin{cases} G_{22\_Re} = G_{22} + \mathrm{Re}(\overline{S}_{20}(\overline{W}_2[0])^2) & G_{33\_Re} = G_{33} + \mathrm{Re}(D[0]) \\ B_{22\_Re} = B_{22}\text{-}\mathrm{Im}(\overline{S}_{20}(\overline{W}_2[0])^2) & B_{33\_Re} = B_{33}\text{-}\mathrm{Im}(D[0]) \\ G_{22\_Im} = G_{22}\text{-}\mathrm{Re}(\overline{S}_{20}(\overline{W}_2[0])^2) & G_{33\_Im} = G_{33}\text{-}\mathrm{Re}(D[0]) \\ B_{22\_Im} = B_{22} + \mathrm{Im}(\overline{S}_{20}(\overline{W}_2[0])^2) & B_{33\_Im} = B_{33} + \mathrm{Im}(D[0]) \end{cases} \tag{21}$$

As shown in Fig. 5, DPRHEM is structured into three distinct steps: *Step* 1: When there is an initial voltage estimation (e.g., case13659pegase system in start-up mode 1), the initial voltage estimate is directly used as the initialized "germ" and enters *Step* 3. When there is no initial voltage estimation, it is necessary to construct a classical HEM initialization model. When the initialized classical HEM model s = 0, it corresponds to the no-load state, and can obtain physically meaningful solutions that are easy to solve. All bus voltages are 1p.u., and all power states are 0p.u.. The classical HEM model is constructed with reference [12], n = 0, the number of restarts of the model m = 0, and transfers to *Step* 2.

Step 2: The power series coefficient of the HEM model is calculated order by order (n++). If $\Delta S_n < \varepsilon$, the power flow converges. If n > 100 or m > 10, the power flow cannot converge, and there is no need

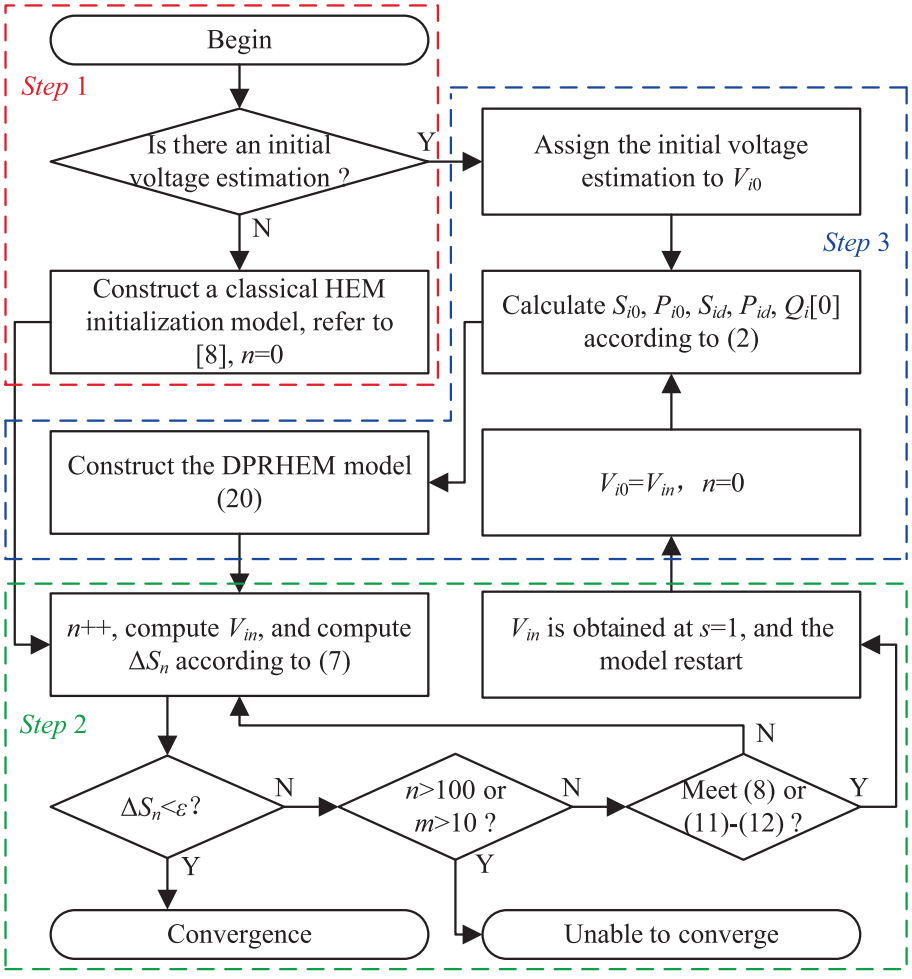

Fig. 5. Flowchart of the DPRHEM.

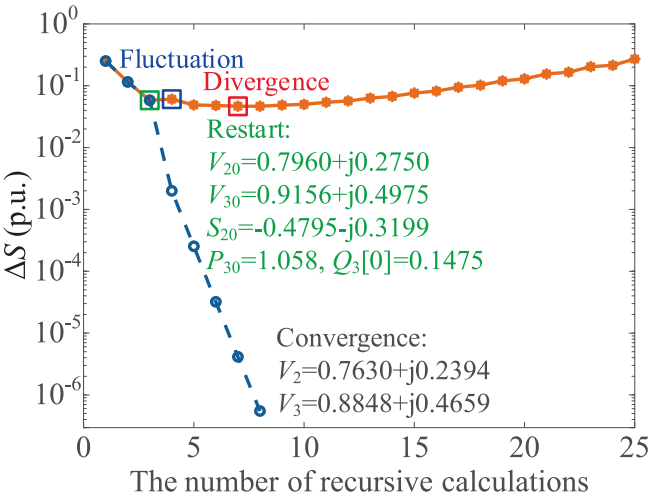

Fig. 6. A tutorial example of 3-bus system.

to restart and end the cycle. If the change trend of ΔS_n satisfies (8) or (11)-(12), the V_{in} at s = 1 is obtained and the model restarts and enters *Step* 3.

Step 3: Let $V_{i0} = V_{in}$, n = 0 of the restarted model, the initial state power $S_{i0}(P_{i0})$ and the direction correction power S_{id} (P_{id}) are calculated according to (2). According to (20), the DPRHEM model after restart is constructed (when the case13659pegase is system in start-up mode 1, the initial voltage estimation from the MATPOWER data file is directly assigned to V_{i0} to realize the DPRHEM model construction). Return to *Step* 2.

The 3-bus system data shown in Fig. 4 is derived from [21]. Taking this as a tutorial example, we introduce the proposed method steps under the condition that the convergence accuracy ε is set to 10^{-6}. Fig. 6 shows that the classical HEM cannot converge, and begins to fluctuate after calculating the 4-order coefficient, and begins to diverge after calculating the 7-order coefficient. DPRHEM only needs to perform 1 restart to calculate a total of 8-order coefficients to achieve convergence. When the 3-order coefficient calculation is completed in the classical HEM, the DPRHEM can perform the first restart through Steps 1 and 2. Then, based on the initial state passed in Step 2, Step 3 is executed to realize the restart and update of the DPRHEM model, and then back to Step 2, and the convergence is realized after the 5-order coefficient calculation is continued. The initial state at restart and the final convergence results are shown in Fig. 6. It can be observed that the proposed method restarts after the classical HEM performs the 3-order calculation, which avoids the fluctuation phenomenon of the classical HEM in the 4-order and the divergence phenomenon in the 7-order, and effectively improves the convergence performance of the HEM.

4. Case study

4.1. Test system setting

In this section, the accuracy, computational efficiency, and convergence of four power flow methods: the DPRHEM, the classical HEM, the NRM, and the RHELM power flow methods are compared and analyzed. The convergence accuracy ε of power flow calculations is set to 1×10^{-6}p.u. for all test cases. The evaluations were conducted on a personal computer equipped with a 12th Generation Intel (R) Core (TM) i9-12900H operating at approximately 2.5 GHz, with 16 GB of memory. MATLAB R2022b served as the software platform. The following three systems (Simple analysis of the applicability of other systems is shown in Appendix) were selected to benchmark the performance of the methods:

1) case9 [44]: This dataset corresponds to a small network consisting of 9 buses and 3 generators.
2) case13659pegase [45,46]: Representing a large-scale European high-voltage transmission network, this system contains 13,659 buses, 4,092 generators, and 20,467 branches. It can accurately reflect the complexity and size of the network.
3) East China regional power grid (10082-bus system): Covering five provinces in China, this regional power grid consists of 10,082 buses, including 9,474 PQ buses, 607 PV buses, with 5,796 transformers, and 15,160 branches.

For all systems analyzed, the phase angle influence of transformers was ignored in this paper, setting the phase shift angle to 0. Unless otherwise noted, the maximum degree N of the power series calculation order used in the RHELM (N_0 for the initial run and N_R for restarting) follows the settings from [22]: $N_0 = 2$, $N_R = 6$.

4.2. Accuracy comparison

In order to verify the accuracy of the convergence results of the methods and conduct a comparative analysis, each power system uses the convergence results of the NRM in MTAPOWER as a benchmark. For most systems, this benchmark is drawn from MATPOWER results. However, because the 10082-bus system lacks the data form of MATPOWER, the results of the NRM from the Bonneville Power Administration (BPA) software are used instead. The accuracy of the DPRHEM, classical HEM, and RHELM are compared by evaluating the maximum absolute errors in the electrical parameters after the convergence. The detailed comparisons are shown in Table 2. The load rates of case9 and 10082-bus systems are both 100 %. For the case13659pegase system, two start-up methods are considered: 1) Initial estimate from MATPOWER Data File (the load rate is set as 100 % of the original); 2) and flat start (the load rate I's set as 5 % of the original). In Table 2, the entries labeled "1)" and "2)" represent the start-up mode utilized for each trial. For the flat start mode in the case 13659pegase system, the maximum degree of the RHELM power series calculation order is set to $N_0 = N_R = 6$. The variable λ in Table 2 represents the computational performance of the method, and the expression format is (Number of Restarts, Order of Convergence, Time (s)).

Table 2
Maximum Absolute Errors in Convergence Results.

Method	System Size	λ	$\lvert V\rvert$ (p.u.)	θ (p.u.)	P (p.u.)	Q (p.u.)
DPRHEM	9-bus	(1,5,9.0 × 10^{-5})	3.0 × 10^{-8}	2.7 × 10^{-6}	7.0 × 10^{-8}	4.6 × 10^{-7}
	10082-bus	(3,12, 9.7 × 10^{-2})	4.0 × 10^{-8}	4.6 × 10^{-7}	6.0 × 10^{-7}	5.7 × 10^{-7}
	1) 13659-bus	(3,12,1.4 × 10^{-1})	1.0 × 10^{-8}	3.4 × 10^{-6}	3.5 × 10^{-7}	4.4 × 10^{-7}
	2) 13659-bus	(3,19,1.5 × 10^{-1})	1.0 × 10^{-8}	2.9 × 10^{-7}	2.0 × 10^{-8}	4.0 × 10^{-8}
HEM	9-bus	(/,9, 1.1 × 10^{-4})	2.7 × 10^{-7}	3.8 × 10^{-6}	5.5 × 10^{-7}	2.0 × 10^{-6}
	10082-bus	(/,/,/)	/	/	/	/
	13659-bus	(/,/,/)	/	/	/	/
RHELM	9-bus	(1,6,1.1 × 10^{-4})	1.3 × 10^{-7}	3.4 × 10^{-6}	8.0 × 10^{-8}	1.4 × 10^{-6}
	10082-bus	(4,21,1.4 × 10^{-1})	1.0 × 10^{-7}	4.5 × 10^{-6}	8.0 × 10^{-7}	1.5 × 10^{-6}
	1) 13659-bus	(4,17,2.1 × 10^{-1})	4.7 × 10^{-7}	9.3 × 10^{-6}	3.0 × 10^{-7}	2.5 × 10^{-6}
	2) 13659-bus	(4,21,2.2 × 10^{-1})	1.4 × 10^{-7}	1.8 × 10^{-5}	1.3 × 10^{-6}	1.8 × 10^{-6}

From Table 2, it can be seen that all three methods can converge on the case9 system, with the maximum absolute errors in the convergence results that are minimal, and within the predefined convergence accuracy thresholds. This outcome confirms the efficacy of both the proposed method and the compared methods in terms of accuracy. Further analysis of the results across different sizes of power systems reveals that both the RHELM and the DPRHEM effectively solve the issues that the classical HEM is unable to converge in large-scale power system power flow analyses. The incorporation of the restart strategy significantly enhances their capability to solve power flow convergence problems in such scenarios.

On the other hand, the analysis of the case13659pegase system in two start-up modes is motivated by an interesting observation by the authors. Specifically, it appears that this system displays different load ranges and varying convergence capabilities in different start-up modes. Interestingly, even when the power flow converges under a certain load condition, the results may not necessarily be meaningful. The analysis of this problem will be carried out in greater detail in the next section.

4.3. Convergence analysis

1) Analysis of method convergence across different load ranges

The NRM has varying convergence across different load ranges, depending on the initial values selected. And the HEM's convergence is affected by load rate. In order to analyze this situation more intuitively, this paper examines the convergent load range of the four methods on large systems: case 13659pegase and the East China regional power grid. The analysis is conducted in increments of 1 % load rate, with the findings presented in Fig. 7.

As depicted in Fig. 7, the HEM has difficulty converging in large-scale and heavy-load systems. Although the NRM can converge under various load rates in a large system, the physical significance of its solutions cannot always be guaranteed. The RHELM does ensure physically

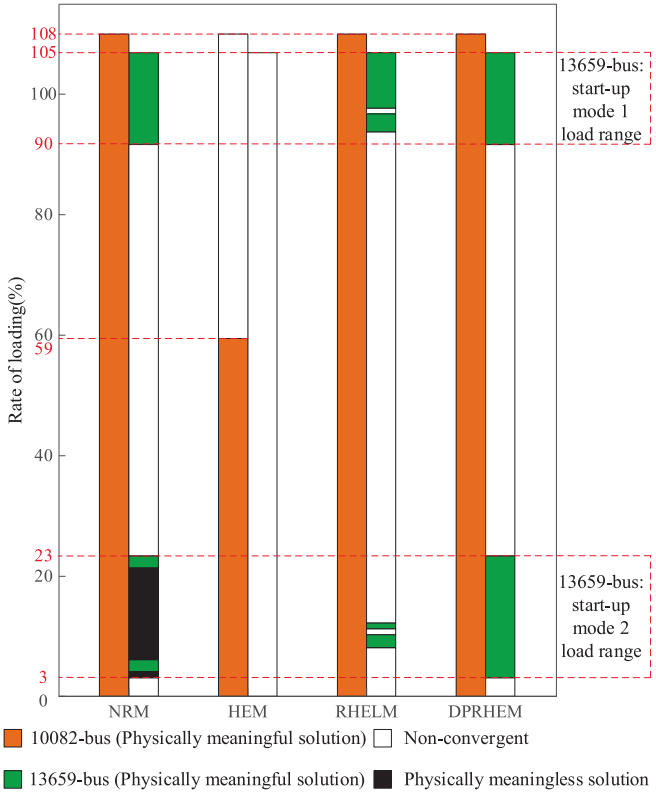

Fig. 7. Convergence of the methods at different load rates.

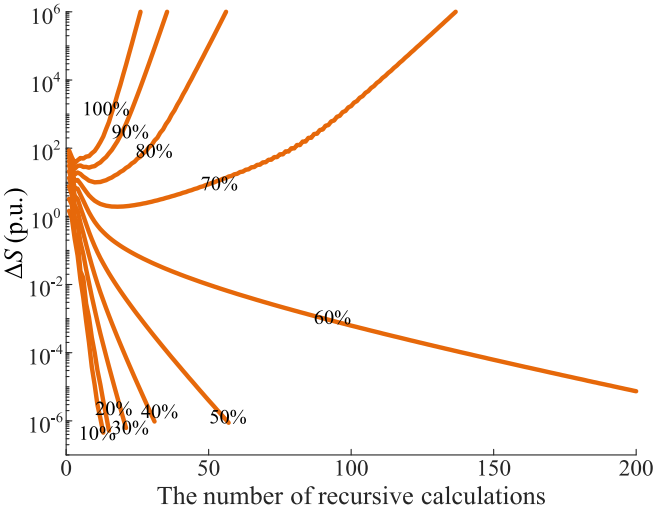

Fig. 8. The change trend of HEM's Δ*S* with load rate.

meaningful solutions under certain load conditions. However, the fixed restart mechanism of RHELM limits its ability to dynamically correct the solution direction, thus affecting its convergence capability across all load ranges on a large system. In contrast, the dynamically restarted DPRHEM can greatly guarantees the maximization of the convergence domain, and the phase angle constraint (12) ensures convergence to physically meaningful solutions in large systems, which has universal applicability. These observations indicate that the dynamic power restart method introduced in this paper effectively corrects the direction of power flow solutions and enhances the reliability of convergence results. At the same time, the case 13659pegase system may have multiple bifurcation points, which makes the above method unable to converge when the case 13659pegase system load rate is 24 %-90 % under the two start-up modes in Fig. 7.

To analyze the convergence challenge under the heavy load scenario of the large power grid, this paper compares the change trend of HEM and ΔS of the interconnection system in East China with the increase of

Table 3
The Influence of N_0 and N_R on Convergence of RHELM.

Start-up Mode	Rate of Loading (%)	Scheme 1	Scheme 2	Scheme 3
1) 13659-bus	4	/	/	/
	5	/	(4,21)	/
	6	/	(4,25)	/
	7	/	(5,26)	/
	8	/	(5,27)	/
	9	(6,31)	(5,29)	/
	10	(6,31)	(6,31)	/
	11	/	(6,31)	/
	12	(6,27)	/	/
	13 ~ 23	/	/	/
2) 13659-bus	91	/	/	/
	92	/	/	(4,24) physically meaningless solution
	93	(6,28)	/	(4,25)
	94	(4,21)	/	(5,30) physically meaningless solution
	95	(5,24)	/	/
	96	/	/	(4,24)
	97	(4,21)	/	(4,23)
	98	(4,17)	/	(3,22)
	99	(4,17)	/	(3,19)
	100 ~ 101	(4,17)	/	(3,18)
	102 ~ 103	(4,17)	/	(3,17)
	104	(4,17)	/	(3,18)
	105	(4,21)	/	(3,22)

load (the step size is 10 %), and obtains the Fig. 8. It can be seen from Fig. 8 that ΔS begins to converge slowly with the increase of HEM load. Then further, when the load rate reaches the critical value of convergence, such as the load rate of 60 %, HEM cannot converge within 200 orders. When the load rate exceeds the critical value of convergence, HEM begins to diverge, and the trend of divergence becomes more and more obvious. In Fig. 7, both DPRHEM and RHEM greatly improve the convergence performance of HEM under heavy load by restarting. It can be seen that it is of great significance to study the restart mechanism of HEM.

Furthermore, regarding the problem of RHELM's inability to guarantee the convergence across all load ranges on the case13659pegase system, this study investigates the influence of varying the maximum degree N of the power series calculation order on convergence of RHELM. We introduce two new schemes: Scheme 2: $N_0 = N_R = 6$ and Scheme 3: $N_0 = 2$, $N_R = 8$. They are compared with the initial setting (Scheme 1: $N_0 = 2$, $N_R = 6$) to evaluate their impact on convergence. The results are presented in Table 3, which formats the data as (Number of Restarts, Order of Convergence).

From Table 3, it can be seen that RHELM shows different convergence behaviors under different N_0 and N_R conditions. Scheme 2 enhances the convergence range of Scheme 1 under startup mode 1, but it fails to converge under startup mode 2. On the other hand, Scheme 3 enables convergence for some load conditions under start-up mode 2, where Scheme 1 cannot, though it still cannot guarantee power flow overall convergence within the convergent load range. Notably, Scheme 3 encounters non-convergence issues under start-up mode 2, such as physically meaningless solutions or other non-convergence situations, especially at load rates of 92 %, 94 %, and 95 %, and it cannot converge under start-up mode 1. In summary, RHELM cannot guarantee the existence of a universally applicable N_0 and N_R, which limits its application scenarios. Under certain conditions, inappropriate N_0 and N_R will lead to RHELM unable to converge or converge to physically meaningless solutions.

In summary, it is necessary to study a universal restart mechanism with dynamic response ability to ensure the convergence of the method. This necessity makes the research findings of this paper particularly valuable. In view of the fact that conventional power flow calculations typically employ a flat start-up, only start-up mode 2 will be considered in subsequent analysis of the case13659pegase system.

2) The effect of the restart mechanism on convergence

To better present the challenges faced by the classical HEM in large systems under heavy loads and to explore how restart mechanisms influence power flow convergence across various scales and loads, this study compares the bus voltage convergence trajectories of the RHELM and the DPRHEM with classical HEM. Specific examples include a) case9 system, bus 9, the load rate is set to 240 %; b) East China regional power grid system, bus 1666, the load rate is 70 %; and c) case13659pegase system, start-up mode 2, Scheme 1, bus 3876, the load rate is 20 %. Observing the change of voltage convergence trajectories after each restart can effectively analyze the performance and reliability of the proposed method, with the results shown in Fig. 9.

Fig. 9 a) shows that in the case9 system, both RHRLM and DPRHEM significantly enhance efficiency by reducing the number of recursive calculations originally required by classical HEM from 83 to 11 and 8 through 2 restarts. This reduction translates to 70 fewer recursive calculations needed to reach convergence and shows the effectiveness of the restart mechanism.

Similarly, Fig. 9 b) shows that in the East China regional power grid system, the RHELM required 3 restarts and a total of 16 recursive calculations to achieve power flow convergence. In contrast, the PRHEM needed only 2 restarts and a total of 9 recursive calculations to converge. These results demonstrate that the restart method effectively mitigates the challenges posed by the classical HEM, particularly its reliance on

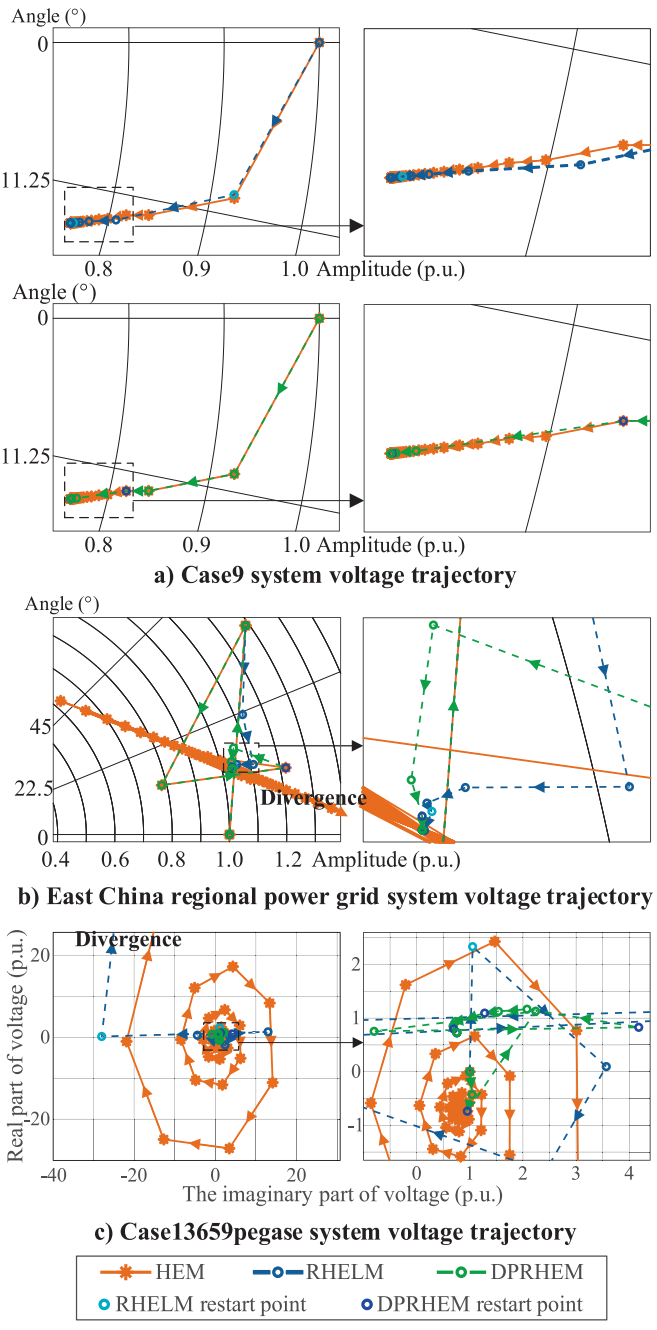

Fig. 9. Voltage convergence trajectories of each method.

multiple recursive calculations to obtain high-order power series coefficients in the face of large-scale and heavily loaded systems and the difficulties in achieving power flow convergence.

Fig. 9 c) illustrates the convergence issues in the case13659pegase system using RHELM. After the initial restart, RHELM requires calculation up to the power series of N_R order to meet the conditions for the next restart. However, the diagram reveals that the voltage of RHELM has a large deviation when restarting. At this time, despite the model restart, solving the divergence issue remains challenging. Conversely, DPRHEM manages to achieve convergence within 5 restarts, through a total of 15 recursive calculations. The figure shows that the first 2 restarts of DPRHEM correct the convergence direction of power flow, while the last 3 restarts accelerate the convergence speed. It can be seen that the DPRHEM's strategy of dynamically correcting the analytical direction based on power changes effectively ensures the reliable

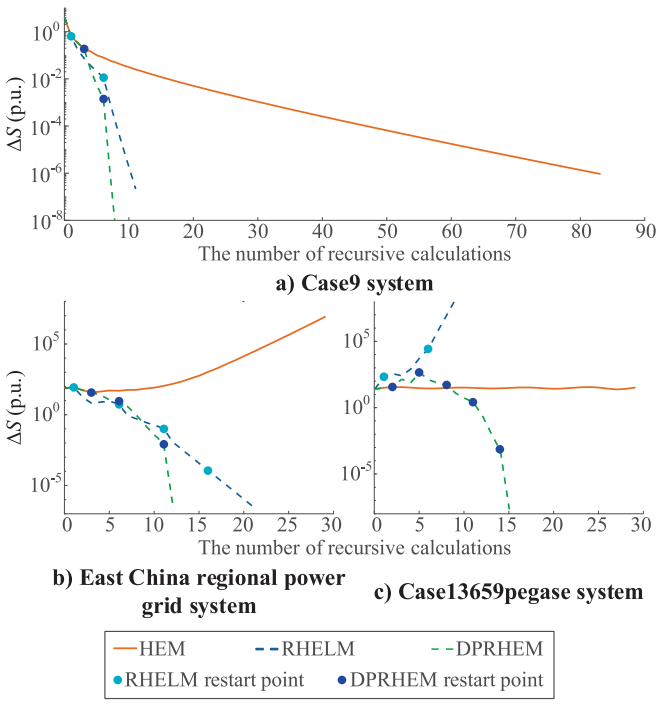

Fig. 10. Changes in the maximum power residual ΔS.

convergence of HEM-type power flow methods.

3) Analysis of power state changes

In the process of power flow calculation, the maximum power residual ΔS is a crucial indicator for assessing whether the power flow converges. The behavior of ΔS can reflect the convergence speed and stability of the method. In this section, the changes in ΔS for the three HEM methods are analyzed across the case9 system, the East China regional power grid, and the case13659pegase system. The results are presented in Fig. 10. Among them, the load rate is set at 240 % for the case9 system, 100 % for the East China regional power grid, and 20 % for the case13659pegase system in the flat start mode.

Fig. 10 a) shows that RHELM and DPRHEM significantly accelerate the reduction of the maximum power residual ΔS after the model restart in the heavily loaded case9 system. It can be seen from Fig. 10 b) that both RHELM and DPRHEM employ a single-model restart to avert the ΔS divergence trend of HEM, thus ensuring the convergence stability of the two methods. Furthermore, both Figs. 10a) and b) highlight the fact that DPRHEM outperforms RHELM in improving the convergence speed of ΔS after each restart. It illustrates the significant impact of restart timing on the computational efficiency of the methods.

Fig. 10c) can reflect the influence of the restart timing on the convergence performance of the algorithm. It can be seen that the divergence trend of ΔS in RHELM becomes increasingly pronounced after two restarts, while DPRHEM effectively corrects the divergence trend through only two restarts. This contrast suggests that without

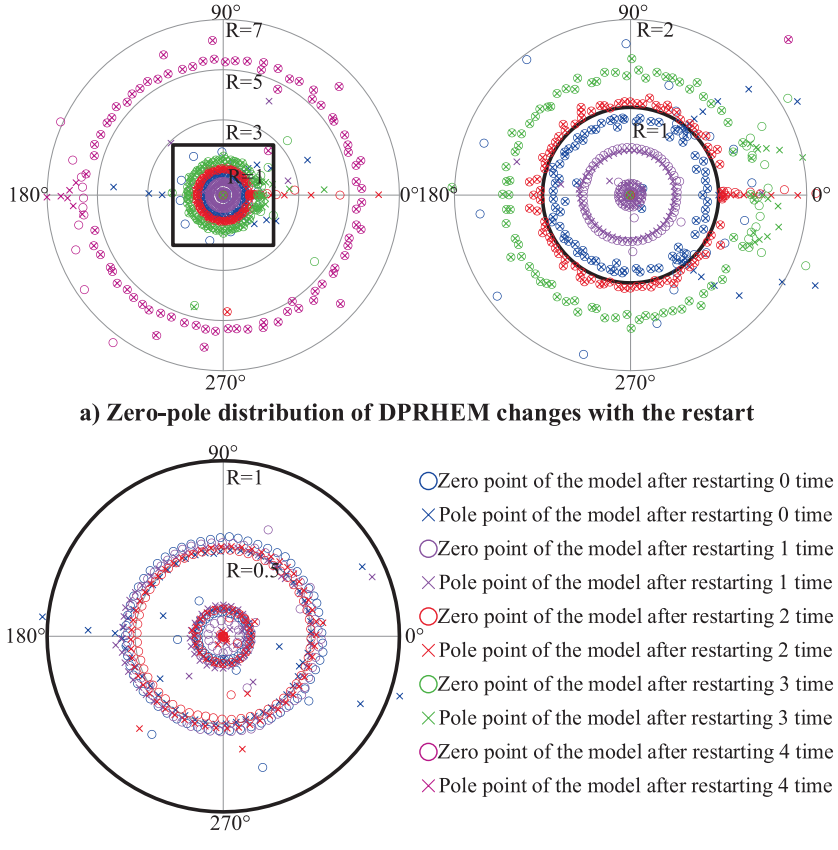

Fig. 11. The distribution of zero and pole of the model.

timely and properly executed restarts, it may not only fail to optimize the convergence performance of the HEM-type power flow methods, but may even induce the divergence trend of these methods in advance, resulting in worse convergence performance. In summary, the restart mechanism proposed in this paper has superior adaptability to different systems. Compared with RHELM, which fixes the maximum degree N of the power series calculation order, DPRHEM demonstrates better convergence and a wider application range.

4) Analysis of model convergence radius

To further verify the improvement of HEM convergence by the proposed method and verify that the restart mechanism of the proposed method is better than RHELM, this example is under the condition of Fig. 9 c), RHELM and DPRHEM calculate the 200-order coefficient after each restart, and then perform Padé approximation and plot the zero-pole distribution to obtain Fig. 11. Fig. 11 a) shows the process of the zero-pole distribution of DPRHEM changing with the restart. The right figure is the local amplification in the left figure box. Fig. 11 b) shows the process of the zero-pole distribution of RHELM changing with the restart. Since DPRHEM is initialized by HEM, the zero-pole distribution of classical HEM can be represented by the zero-pole distribution of DPRHEM restarted 0 times in Fig. 11 a).

Fig. 11 a) shows that the convergence radius of DPRHEM without restart (HEM) is less than 1 and the method cannot converge. After DPRHEM performs 1 restart, the convergence radius becomes smaller, the convergence is worse, and the method cannot converge. However, after performing 2 restarts, the convergence radius is approximately close to 1 and the method can converge at this time. However, the calculation of high-order power series coefficients is still needed and the convergence is slow. A total of 2 restarts and 345-order calculations are required. After 3 restarts, the convergence radius is about 1.5, which is more than 1, and the convergence speed of the model is accelerated. A total of 3 restarts and 50-order calculations are required. After 4 restarts, the convergence radius is about more than 5 and the convergence speed of the model is very fast. A total of 4 restarts and 18-order calculations are required. Fig. 11 b) shows that the fixed restart mechanism of RHELM does not change the convergence radius of the algorithm and cannot converge under the current operating conditions. It can be seen that the dynamic restart mechanism of the proposed method is more applicable than the fixed restart mechanism of RHELM. Moreover, the dynamic restart mechanism of the proposed method can expand the convergence radius and effectively deal with the problem of classical HEM convergence difficulty. For the case where the convergence radius becomes smaller after one restart of DPRHEM, the authors believe that the reason is that it is difficult to obtain high-quality restart points under constraints (11) and (12) during the model divergence process. In this regard, it is hoped that it can be improved in the follow-up study.

Table 4
Iterative Solution Time and Recursive Solution Time.

Time Consumed (s)	System Size	NRM	HEM	RHELM	DPRHEM
Matrix Decomposition	9-bus	2.05×10^{-5}	1.96×10^{-5}	2.15×10^{-5}	2.01×10^{-5}
	10082-bus	2.04×10^{-2}	1.99×10^{-2}	2.08×10^{-2}	1.99×10^{-2}
	13659-bus	3.77×10^{-2}	3.50×10^{-2}	4.23×10^{-2}	3.71×10^{-2}
Back Substitution	9-bus	1.00×10^{-5}	1.00×10^{-5}	1.07×10^{-5}	1.00×10^{-5}
	10082-bus	1.45×10^{-3}	1.48×10^{-3}	1.52×10^{-3}	1.43×10^{-3}
	13659-bus	2.17×10^{-3}	2.10×10^{-3}	2.44×10^{-3}	2.15×10^{-3}

4.4. Efficiency of method calculations

All the methods in this paper use LU decomposition to solve the equation, which mainly includes matrix decomposition and back substitution. Next, the calculation complexity and calculation cost of all methods will be analyzed based on LU decomposition. To evaluate the efficiency of the proposed method, the Intel® oneAPI Math Kernel Library (oneMKL) PARDISO solver is used to solve the sparse matrix linear equations. Specifically, we measure the time required for NRM, classical HEM, RHELM, and DPRHEM to perform matrix decomposition in each test system and the time required for each test system to perform back substitution calculations using the LU decomposition matrix. The results are averaged after 100 times of calculation. The results are compiled and shown in Table 4.

From Table 4, it is evident that the time required for matrix decomposition considerably exceeds the time needed for matrix back-substitution calculation. This disparity is more obvious in large-scale systems. As observed in case13659pegase and East China regional power grid systems, the time required for matrix decomposition is about 13 to 18 times that for matrix back substitution calculations. This is because in LU decomposition of power flow calculation, the computational complexity of matrix decomposition is $O(n^3)$, and the computational complexity of back substitution is $O(n^2)$ [47]. Therefore, the time consumed by one matrix decomposition is more than the time consumed by one back substitution. In summary, when the cumulative time required for the back substitution is more than the time required for one matrix decomposition, the restart mechanism is used to balance the number of matrix decompositions and the number of back substitutions, which can avoid redundant back substitution times and effectively improve the computational efficiency of the method.

When the NRM is used to perform power flow calculation, each iteration necessitates one matrix decomposition and one back substitution. Unlike NRM, the classical HEM requires only one matrix decomposition, and then each next-order power series coefficient is calculated. Only one back substitution operation needs to be performed. This is because the matrix A remains unchanged in the recursive calculation process. Both the RHELM and the DPRHEM are improvements over the HEM. However, they need to perform an additional matrix decomposition upon each restart. Therefore, an unreasonable restart mechanism may run the risk of reducing computational efficiency. In summary, the computational complexity of DPRHEM and RHELM is m*O($8N^3$) + n*O($4N^2$). The computational complexity of HEM isO($8N^3$) + n*O($4N^2$). The computational complexity of NRM is n*(O($8N^3$) + O($4N^2$)). m is the number of restarts of DPRHEM or RHELM, and n is the total order of calculation when the HEM method converges (for NRM, n represents the number of iterations). To further evaluate the computational efficiency of the four methods under different operating conditions, this paper compares the calculation times required by the case9, East China regional power grid and case13659pegase systems under different load rates, and obtains Table 5.

The analysis of the case9 system shows that the HEM demonstrates higher computational efficiency than the NRM when the load rates are low. However, as the system load rate increases, the HEM requires calculations over high-order convergence series, which in turn results in a decrease in computational efficiency. Both the RHELM and the DPRHEM optimize the computational efficiency of the HEM by implementing restart mechanisms and address the convergence challenges faced by HEM in large-scale and heavily loaded systems. Table 5 shows that DPRHEM's restart mechanism is more effective than that of RHELM, leading to a slightly better computational efficiency than RHELM. Comparative analysis across different operational conditions and systems consistently confirms the superior computational efficiency of DPRHEM over that of NRM, HEM, and RHELM. Although the improvement of the computational efficiency of the proposed method is not obvious for engineering application of cross-section power flow

Table 5
Comparison of Calculation Times for DPRHEM, NRM, HEM, and RHELM.

System Size	Rate of Loading (%)	NRM		HEM		RHELM			DPRHEM		
		Number of Iterations	Time (s)	Order of Convergence	Time (s)	Order of Convergence	Number of Restarts	Time (s)	Order of Convergence	Number of Restarts	Time (s)
9-bus	20	3	9.2×10^{-5}	5	7.0×10^{-5}	6	1	1.1×10^{-4}	4	1	8.0×10^{-5}
	40	3	9.2×10^{-5}	6	8.0×10^{-5}	4	1	8.6×10^{-5}	4	1	8.0×10^{-5}
	60	3	9.2×10^{-5}	7	9.0×10^{-4}	6	1	1.1×10^{-4}	4	1	8.0×10^{-5}
	80	3	9.2×10^{-5}	8	1.0×10^{-4}	6	1	1.1×10^{-4}	5	1	9.0×10^{-5}
	100	3	9.2×10^{-5}	9	1.1×10^{-4}	6	1	1.1×10^{-4}	5	1	9.0×10^{-5}
	120	4	1.2×10^{-4}	11	1.3×10^{-4}	7	2	1.4×10^{-4}	5	1	9.0×10^{-5}
	140	4	1.2×10^{-4}	14	1.6×10^{-4}	7	2	1.4×10^{-4}	6	1	1.0×10^{-4}
	160	4	1.2×10^{-4}	17	1.9×10^{-4}	8	2	1.5×10^{-4}	6	1	1.0×10^{-4}
	180	4	1.2×10^{-4}	23	2.5×10^{-4}	8	2	1.5×10^{-4}	7	1	1.1×10^{-4}
	200	4	1.2×10^{-4}	31	3.3×10^{-4}	9	2	1.6×10^{-4}	7	1	1.1×10^{-4}
	220	5	1.5×10^{-4}	46	4.8×10^{-4}	11	2	1.8×10^{-4}	8	2	1.4×10^{-4}
	240	5	1.5×10^{-4}	83	8.5×10^{-4}	11	2	1.8×10^{-4}	8	2	1.4×10^{-4}
10082-bus	20	4	8.7×10^{-2}	15	4.2×10^{-2}	11	2	7.9×10^{-2}	15	0	4.1×10^{-2}
	40	5	1.1×10^{-1}	31	6.6×10^{-2}	12	3	1.0×10^{-1}	8	1	5.1×10^{-2}
	60	5	1.1×10^{-1}	/	/	14	3	1.0×10^{-1}	13	1	5.8×10^{-2}
	80	6	1.3×10^{-1}	/	/	17	4	1.3×10^{-1}	11	2	7.5×10^{-2}
	100	7	1.5×10^{-1}	/	/	21	4	1.4×10^{-1}	12	3	9.7×10^{-2}
1) 13659-bus	5	6	2.4×10^{-1}	/	/	/	/	/	19	3	1.9×10^{-1}
	10	5	physically meaningless solution	/	/	31	6	3.7×10^{-1}	10	3	1.7×10^{-1}
	15	5		/	/	/	/	/	14	3	1.8×10^{-1}
	20	6		/	/	/	/	/	15	5	2.5×10^{-1}
2) 13659-bus	95	5	2.0×10^{-1}	/	/	24	5	3.1×10^{-1}	17	5	2.6×10^{-1}
	100	5	2.0×10^{-1}	/	/	17	4	2.5×10^{-1}	12	3	1.7×10^{-1}
	105	6	2.4×10^{-1}	/	/	21	4	2.6×10^{-1}	15	5	2.5×10^{-1}

analysis. However, when faced with the need to perform a large number of power flow calculation operations in a short time (such as fast security analysis of power grid [48], uncertain power flow probability analysis [49], etc.), the proposed method may be more easier to show more obvious efficiency improvement. At the same time, the proposed method is more likely to reflect higher efficiency [48,50,51] after combining high-performance computing platforms such as CPU-GPU.

5. Conclusion

In this paper, a DPRHEM power flow method based on power restart is proposed to address the convergence issues experienced by the HEM power flow method for large-scale and heavily loaded power grids. DPRHEM introduces a restart mechanism based on the changes in the maximum power residual ΔS as the restart update criterion, which effectively overcomes the poor convergence of HEM under large-scale and heavily loaded power grids. This approach not only clarifies the physical basis of the restart mechanism, but also enhances the stability and computational efficiency of the convergence process. In contrast to the RHELM, which sets a fixed maximum degree N for the power series calculation order, DPRHEM's restart mechanism makes it suitable for a broader range of applications. DPRHEM can better cope with the problem that the power flow cannot be reliably converged in ill-conditioned operation scenarios (for example, the load growth is too fast and the power flow calculation is difficult to converge due to large-scale system integration).

The proposed method belongs to the exploratory study on the dynamic restart mechanism. Although the content of the proposed method has been improved, and the convergence is better than HEM, NRM and RHELM in the test case, it can meet the application requirements in engineering. However, it is difficult to prove the reliability of the "germ" transmitted when the proposed method restarts through strict mathematical principles. The mathematical theory of the restart mechanism in HEM still needs to be further proved to improve the interpretability of the method. The fault-tolerant mechanism considering a certain margin for restart constraints may improve the robustness of the method in ill-conditioned system power flow analysis, and then improve the adaptability of the proposed method in power system applications. These will be the focus of the author's future research.

CRediT authorship contribution statement

Yi Zhang: Methodology, Conceptualization. **Tian Lan:** Writing – review & editing, Writing – original draft, Validation, Software. **Chuandong Li:** Visualization. **Weijie Cai:** Investigation. **Zhiyu Lin:** Supervision.

Declaration of competing interest

The authors declare that they have no known competing financial interests or personal relationships that could have appeared to influence the work reported in this paper.

Appendix

The convergence order of DPRHEM, HEM and RHELM proposed under different systems is analyzed. The results are shown in the Table R1 to verify the applicability of the proposed method.

Table R1
Calculation Results of Different Scale Systems.

System	HEM	RHELM	DPRHEM
case9	9	(1,6)	(1,5)
case33	6	(1,4)	(1,4)
regional grid (1152-bus)	186	(3,14)	(2,10)
case2868rte	/	(2,11)	(2,11)
East China regional power grid (10082-bus)	/	(4,21)	(3,12)
case13659pegase	/	(4,17)	(3,12)

It can be noted that in small-scale systems, such as case9 and case33 systems, the improvement of convergence performance is not obvious. In medium and large-scale systems (such as regional grid, case2868rte, East China regional power grid, case13659pegase), the improvement effect of the proposed restart method is very obvious, which can deal with the problem that the classical HEM is difficult to converge.

Data availability

The authors do not have permission to share data.

References

[1] Zimmerman RD, Murillo-Sánchez CE, Thomas RJ. MATPOWER: steady-state operations, planning, and analysis tools for power systems research and education. IEEE Trans Power Sys 2011;26(1):12–9.
[2] Zhang Y, Lin J, Li C. A three-phase power flow algorithm for ungrounded network based on constraints of zero-sequence components. Int Electr Power Energy Syst 2022;145. 108676.
[3] Zhang F, Cheng CS. A modified Newton method for radial distribution system power flow analysis. IEEE Trans Power Sys 1997;12(1):389–97.
[4] Tortelli OL, Lourenço EM, Garcia AV, Pal BC. Fast decoupled power flow to emerging distribution systems via complex pu normalization. IEEE Trans Power Sys 2015;30(3):1351–8.
[5] Zhang W, et al. Spatial-temporal resilience assessment of distribution systems under typhoon coupled with rainstorm events. IEEE Trans Ind Inf 2025;21(1):188–97.
[6] Yang H, Zhang C, Li J, Zhu L, Zhou K. A Novel robust energy storage planning method for grids with wind power integration considering the impact of hurricanes. IEEE Trans Sustain Energy 2025;16(2):1388–400.
[7] Wang D, et al. A novel interval power flow method based on hybrid box-ellipsoid uncertain sets. IEEE Trans Power Sys 2024;39(4):6111–4.
[8] Zhang C, Chen H, Ngan H, Yang P, Hua D. A mixed interval power flow analysis under rectangular and polar coordinate system. IEEE Trans Power Sys 2017;32(2):1422–9.
[9] Liu Z, Zhang X, Su M, Sun Y, Han H, Wang P. Convergence analysis of newton-raphson method in feasible power-flow for DC network. IEEE Trans Power Sys 2020;35(5):4100–3.
[10] Liu Z, et al. Further results on newton-raphson method in feasible power-flow for DC distribution networks. IEEE Trans Power Del 2022;37(2):1348–51.
[11] Sun Q, Liu L, Ma D, Zhang H. The initial guess estimation newton method for power flow in distribution systems. IEEE/CAA J Automatic 2017;4(2):231–42.
[12] A. Trias. The holomorphic embedding load flow method. 2012 IEEE Power and Energy Soc. General Meeting (PESGM), San Diego, CA, USA, 2012, pp. 1-8.
[13] Ma H, Liu C, Zhao H, Zhang H, Wang M, Wang X. A novel analytical unified energy flow calculation method for integrated energy systems based on holomorphic embedding. Appl Energy 2024;15(3):1677–89.

[14] Lima G, de Melo I, Filho J. Interval holomorphic embedding load flow method: a novel approach for interval analysis considering load and generation uncertainties. Electr Power Syst Res 2024;226. 109921.
[15] Sayed AR, Zhang X, Wang G, Wang C, Qiu J. Optimal operable power flow: sample-efficient holomorphic embedding-based reinforcement learning. IEEE Trans Power Sys 2024;39(1):1739–51.
[16] Morgan MY, Shaaban MF, Sindi HF, Zeineldin HH. A holomorphic embedding power flow algorithm for islanded hybrid AC/DC microgrids. IEEE Trans Smart Grid 2022;13(3):1813–25.
[17] Sun Q, Zhang Y, Zhou Y, Wang J, Wang J. Multi-dimensional holomorphic embedding three-phase power flow for AC-DC hybrid distribution systems. IEEE Trans Power Sys 2024;39(3):5310–23.
[18] Zhao Y, Li C, Ding T, Hao Z, Li F. Holomorphic embedding power flow for AC/DC hybrid power systems using bauer's eta algorithm. IEEE Trans Power Sys 2021;36 (4):3595–606.
[19] Sun Y, Ding T, Han O, Liu C, Li F. Static voltage stability analysis based on multi-dimensional holomorphic embedding method. IEEE Trans Power Sys 2023;38(4): 3748–59.
[20] Sun Y, Ding T, Qu M, Wang F, Shahidehpour M. Interval total transfer capability for mesh HVDC systems based on sum of squares and multi-dimensional holomorphic embedding method. IEEE Trans Power Sys 2022;37(6):4157–67.
[21] Chiang HD, Wang T, Sheng H. A novel fast and flexible holomorphic embedding power flow method. IEEE Trans Power Syst 2018;33(3):2551–62.
[22] Freitas FD, et al. Restarted holomorphic embedding load-flow model based on low-order Padé approximant and estimated bus power injection. Int Electr Power & Energy Syst 2019;112:326–38.
[23] Á. B. Domínguez, F. M. Echavarren and L. Rouco. A convergence control scheme for multi-stage holomorphic embedding load-flow method. IEEE Trans. Power Syst., early access, doi: 10.1109/TPWRS.2024.3401782.
[24] Zhang W, Wang T, Chiang H-D. A novel FFHE-inspired method for large power system static stability computation. IEEE Trans Power Syst 2022;37(1):726–37.
[25] W. Zhang, Y. Zhang, C. Zhang, H. -D. Chiang and T. Wang. A robust holomorphic embedding-based method for fast tracing of P-V curves with limiting points. IEEE Trans Power Syst., early access, doi: 10.1109/TPWRS.2025.3560892.
[26] Hopkins TR. On the sensitivity of the coefficients of Padé approximants with respect to their defining power series coefficients. J Comput Appl Math 1982;8(2): 105–9.
[27] Rao S, Feng Y, Tylavsky D, Subramanian M. The holomorphic embedding method applied to the power-flow problem. IEEE Trans Power Syst 2016;31(5):3816–28.
[28] Rao S, Tylavsky DJ. Theoretical convergence guarantees versus numerical convergence behavior of the holomorphically embedded power flow method. Int Electr Power Energy Syst 2018;95:166–76.
[29] Li S, Tylavsky D, Shi D, Wang Z. Implications of Stahl's theorems to holomorphic embedding part I: theoretical convergence. CSEE J Power Energy Syst 2021;7(4): 761–72.
[30] Dronamraju A, et al. Implications of Stahl's theorems to holomorphic embedding part II: numerical convergence. CSEE J Power Energy Syst 2021;7(4):773–84.
[31] Wang T, Chiang HD. On the holomorphic and conjugate properties for holomorphic embedding methods for solving power flow equations. IEEE Trans Power Syst 2020;35(4):2506–15.
[32] Trias A, Marín JL. A Padé-Weierstrass technique for the rigorous enforcement of control limits in power flow studies. Int Electr Power Energy Syst 2018;99:404–18.
[33] Beckermann B, Matos AC. Algebraic properties of robust Padé approximants. J Approx Theory 2015;190:91–115.
[34] Liu C, Wang B, Hu F, Sun K, Bak C. Online voltage stability assessment for load areas based on the holomorphic embedding method. IEEE Trans Power Syst 2018; 33(4):3720–34.
[35] Trias A. Fundamentals of the holomorphic embedding load-flow method. arXiv: 1509.02421 2015.
[36] Weinhold R, Mieth R. Fast security-constrained optimal power flow through low-impact and redundancy screening. IEEE Trans Power Syst 2020;35(6):4574–84.
[37] Fan Z, Yang Z, Yu J, Xie K, Yang G. Minimize linearization error of power flow model based on optimal selection of variable space. IEEE Trans Power Syst 2021;36 (2):1130–40.
[38] Tostado-Véliz M, Alharbi T, Alrumayh O, Kamel S, Jurado F. A novel power flow solution paradigm for well and Ill-conditioned cases. IEEE Access 2021;9: 112425–38.
[39] Milano F. Continuous Newton's method for power flow analysis. IEEE Trans Power Syst 2009;24(1):50–7.
[40] Almeida KC, Kocholik A. Solving Ill-posed optimal power flow problems via Fritz-John optimality conditions. IEEE Trans Power Syst 2016;31(6):4913–22.
[41] Ortega JM, Rheinboldt WC. Rates of Convergence - General. In: Iterative solution of nonlinear equations in several variables. Maryland, USA: Academic Press; 1970. p. 281–98.
[42] Tostado-Véliz M, Kamel S, Jurado F. Two efficient and reliable power-flow methods with seventh order of convergence. IEEE Syst J 2021;15(1):1026–35.
[43] Zhang Y, Lan T, Li C, Cai W, Lin Z. Holomorphic embedding method based three-phase power flow algorithm considering the sensitivity of the initial value. Int Electr Power Energy Syst 2024;162. 110271.
[44] Chow JH. Time-scale modeling of dynamic networks with applications to power systems. Part of the LNCIS. Springer-Verlag; 1982.
[45] C. Josz, S. Fliscounakis, J. Maeght, and P. Panciatici. AC Power Flow Data in MATPOWER and QCQP Format: iTesla, RTE Snapshots, and PEGASE. https://arxiv.org/abs/1603.01533.
[46] Fliscounakis S, Panciatici P, Capitanescu F, Wehenkel L. Contingency ranking with respect to overloads in very large power systems taking into account uncertainty, preventive and corrective actions. IEEE Trans Power Syst 2013;28(4):4909–17.
[47] Shabat G, Shmueli Y, Aizenbud Y, Averbuch A. Randomized LU decomposition. Appl Comput Harmon Anal 2018;44(2):246–72.
[48] Chen W, Xu J, Wang K. GPU-accelerated N-1 static security analysis based on fine-grained parallelism HELM. Int Electr Power Energy Syst 2022;141. 108074.
[49] Su C, Liu C, Jiang S, Wang Y. Probabilistic power flow for multiple wind farms based on RVM and holomorphic embedding method. Int Electr Power Energy Syst 2021;130. 106843.
[50] Liu C, Qin N, Sun K, Sun K, Bak CL. Remote voltage control using the holomorphic embedding load flow method. IEEE Trans Smart Grid 2019;10(6):6308–19.
[51] Li X, Gao X, Jiang T, Wang C, Li G. Parallel computing method of power system holomorphic embedded power flow. Trans China Electrotech Soc 2024;39(18): 5839–54.